International Journal of Modern Physics B
Vol. 23, No. 9 (2009) 2149–2157

World Scientific
www.worldscientific.com

COUPLING-INDUCED SPIKING COHERENCE IN COUPLED SUBTHRESHOLD NEURONS

WOOCHANG LIM

Neuroscience Laboratory, Institute for Medical Sciences,
Ajou University School of Medicine, Suwon 443-721, Korea
wclim@kangwon.ac.kr

SANG-YOON KIM*

Department of Physics, Kangwon National University,
Chunchon, Kangwon-Do 200-701, Korea
**Department of Physics, University of Wisconsin-Milwaukee,*
P.O. Box 413, Wisconsin 53211, USA
sykim@kangwon.ac.kr

Received 6 January 2009

We consider a large ensemble of globally coupled subthreshold Morris–Lecar neurons. We numerically investigate collective coherence of noise-induced spikings by varying the coupling strength J. As J passes a lower threshold, a transition to collective spiking coherence, which is described in terms of an order parameter, occurs because the coupling stimulates coherence between noise-induced spikings. However, when passing a higher threshold, the coupling induces oscillator death (i.e., quenching of noise-induced spikings) because each neuron is attracted to a noisy equilibrium state. Through competition of these two different roles of coupling, coupling-induced spiking coherence is found to occur in a large range of intermediate coupling strength. The degree of spiking coherence is well-characterized in terms of a coherence measure reflecting the degree of "resemblance" of the global potential to the local potential.

Keywords: Coupled subthreshold neurons; coupling-induced spiking coherence.

PACS numbers: 87.19.L-, 05.40.Ca

1. Introduction

Recently, much attention has been paid to brain rhythms.[1] Synchronous firings in neural systems are correlated with neural encoding of sensory stimuli (e.g., visual binding).[2] Collective dynamics has been intensively investigated in coupled systems, consisting of spontaneously firing (i.e., self-oscillating) neurons, and thus three types of mechanisms for neural synchronization have been found.[3] In contrast to the suprathreshold case of self-oscillating neurons, the case of subthreshold neurons

*Corresponding author.

has received little attention. For an isolated single case, each subthreshold neuron cannot fire spontaneously without noise; it can fire only with the help of noise. Hence, intensive investigation of subthreshold neurons is necessary to understand their coherent collective dynamics.

This paper is organized as follows. In Sec. 2, we consider a large ensemble of globally coupled subthreshold Morris–Lecar (ML) neurons.[4–6] By varying the coupling strength J, we investigate collective coherence of noise-induced spikings. For small J, the global output signal (i.e., the ensemble-averaged membrane potential) becomes incoherent because neurons fire independently. However, as J passes a lower threshold J_l^*, the global output signal becomes coherent (i.e., a transition to spiking coherence occurs) because the coupling stimulates collective coherence between noise-induced spikings. As in globally coupled chaotic systems,[7–10] this coherent transition may be described in terms of the order parameter which is just the mean square deviation of the global output signal. Furthermore, we characterize the degree of spiking coherence by using a coherence measure M reflecting the degree of "resemblance" of the global potential to the local potential. As J is increased from J_l^*, M increases, it becomes maximal at an optimal coupling strength J^*, and then it decreases abruptly. Such an abrupt decrease in M results from the effect of oscillator death (i.e., quenching of noise-induced spikings) occurring for large J.[11–15] This coupling-induced oscillator death, leading to a nonfiring state, occurs because each neuron is attracted to a noisy equilibrium state. As a result of competition of these two different roles of coupling, coupling-induced coherent states appear in a large range of intermediate coupling strength. Finally, a summary is given in Sec. 3.

2. Coupling-Induced Spiking Coherence in Globally Coupled Subthreshold Neurons

We consider a system of N globally coupled neurons. As an element in our coupled system, we choose the conductance-based ML neuron model, originally proposed to describe the time-evolution pattern of the membrane potential for the giant muscle fibers of barnacles.[4–6] The population dynamics in this neural network is governed by a set of the following differential equations:

$$C\frac{dV_i}{dt} = -I_{\text{ion},i} + I_{DC} + D\xi_i + I_{\text{syn},i}\,, \tag{1a}$$

$$\frac{dw_i}{dt} = \phi\frac{(w_\infty(V_i) - w_i)}{\tau_R(V_i)}\,, \quad i = 1, \ldots, N\,, \tag{1b}$$

where

$$I_{\text{ion},i} = I_{\text{Ca},i} + I_{K,i} + I_{L,i} \tag{2a}$$

$$= g_{\text{Ca}} m_\infty(V_i)(V_i - V_{\text{Ca}}) + g_K w_i(V_i - V_K) + g_L(V_i - V_L)\,, \tag{2b}$$

$$I_{\mathrm{syn},i} = \frac{J}{N-1} \sum_{j(\neq i)}^{N} \Theta(V_j - V^*)\,, \tag{2c}$$

$$m_\infty(V) = 0.5[1 + \tanh\{(V - V_1)/V_2\}]\,, \tag{2d}$$

$$w_\infty(V) = 0.5[1 + \tanh\{(V - V_3)/V_4\}]\,, \tag{2e}$$

$$\tau_R(V) = 1/\cosh\{(V - V_3)/(2V_4)\}\,. \tag{2f}$$

Here, the state of the ith neuron at a time t (measured in units of ms) is characterized by two state variables: the membrane potential V_i (measured in units of mV) and the slow recovery variable w_i representing the activation of the K^+ current (i.e., the fraction of open K^+ channels). In Eq. (1a), C represents the capacitance of the membrane of each neuron, and the time evolution of V_i is governed by four kinds of source currents.

The total ionic current $I_{\mathrm{ion},i}$ of the ith neuron consists of the calcium current $I_{\mathrm{Ca},i}$, the potassium current $I_{K,i}$, and the leakage current $I_{L,i}$. Each ionic current obeys Ohm's law. The constants g_{Ca}, g_K, and g_L are the maximum conductances for the ion and leakage channels, and the constants V_{Ca}, V_K, and V_L are the reversal potentials at which each current is balanced by the ionic concentration difference across the membrane. Since the calcium current $I_{\mathrm{Ca},i}$ changes much faster than the potassium current $I_{K,i}$, the gate variable m_i for the Ca^{2+} channel is assumed to always take its saturation value $m_\infty(V_i)$. On the other hand, the activation variable w_i for the K^+ channel approaches its saturation value $w_\infty(V_i)$ with a relaxation time $\tau_R(V_i)/\phi$, where τ_R has a dimension of ms and ϕ is a (dimensionless) temperature-like time scale factor.

Each ML neuron is also stimulated by the common DC current I_{DC} and an independent Gaussian white noise ξ [see the second and third terms in Eq. (1a)] satisfying $\langle \xi_i(t) \rangle = 0$ and $\langle \xi_i(t)\xi_j(t') \rangle = \delta_{ij}\delta(t-t')$, where $\langle \cdots \rangle$ denotes the ensemble average. The noise ξ_i is a parametric one which randomly perturbs the strength of the applied current I_{DC}, and its intensity is controlled by the parameter D. The last term in Eq. (1a) represents the coupling of the network. Each neuron is connected to all the other ones through global instantaneous pulse-type synaptic couplings. $I_{\mathrm{syn},i}$ of Eq. (2c) represents such a synaptic current injected into the ith neuron. The coupling strength is controlled by the parameter J, $\Theta(x)$ is the Heaviside step function (i.e., $\Theta(x) = 1$ for $x \geq 0$ and $\Theta(x) = 0$ for $x < 0$), and V^* is the threshold value for the spiking state (i.e., for $V_i > V^*$ a local spiking state of the ith neuron appears). Here, we consider the excitatory coupling of $J > 0$ and set $V^* = 0$ mV.

The ML neuron may exhibit either type-I or type-II excitability, depending on the system parameters. Throughout this paper, we consider the case of type-II excitability where $g_{\mathrm{Ca}} = 4.4$ mS/cm^2, $g_K = 8$ mS/cm^2, $g_L = 2$ mS/cm^2, $V_{\mathrm{Ca}} = 120$ mV, $V_K = -84$ mV, $V_L = -60$ mV, $C = 5$ μF/cm^2, $\phi = 0.04$, $V_1 = -1.2$ mV, $V_2 = 18$ mV, $V_3 = 2$ mV, and $V_4 = 30$ mV.[16] As I_{DC} passes

a threshold in the absence of noise, each single type-II ML neuron begins to fire with a nonzero frequency which is relatively insensitive to the change in I_{DC}.[17,18] Numerical integration of Eq. (1) is done using the Heun method[19] (with the time step $\Delta t = 0.01$ ms) similar to the second-order Runge–Kutta method, and data for (V_i, w_i) $(i = 1, \ldots, N)$ are obtained with the sampling time interval $\Delta t = 1$ ms. For each realization of the stochastic process in Eq. (1), we choose a random initial point $[V_i(0), w_i(0)]$ for the ith $(i = 1, \ldots, N)$ neuron with uniform probability in the range of $V_i(0) \in (-60, 60)$ and $w_i(0) \in (0.1, 0.5)$.

We consider a large population of globally coupled ML neurons for a subthreshold case of $I_{DC} = 84$ μA/cm^2. For an isolated single case, each subthreshold neuron cannot fire spontaneously in the absence of noise, and it may generate firings only with the aid of noise. We set $D = 1.5$ $\mu\text{A} \cdot \text{ms}^{1/2}/\text{cm}^2$ and numerically investigate collective coherence of noise-induced firings by varying the coupling strength J for $N = 10^3$. Emergence of global spiking coherence in the population may be described by the population-averaged membrane potential $V_G(t)$ (corresponding to the global potential) and the global recovery variable $W_G(t)$,

$$V_G(t) = \frac{1}{N}\sum_{i=1}^{N} V_i(t) \quad \text{and} \quad W_G(t) = \frac{1}{N}\sum_{i=1}^{N} w_i(t)\,. \tag{3}$$

Figure 1(a) shows phase portraits of the global state for three values of J. For small J, neurons fire independently, and hence incoherent states appear. For an incoherent state of $J = 4$ μA/cm^2, the global state lies at a noisy equilibrium point (denoted by an open circle) near $(V_G, W_G) \simeq (-24.8, 0.1)$. However, as J passes a lower threshold J_l^* ($\simeq 6.7$ μA/cm^2), a coherent transition occurs because the coupling stimulates collective coherence between noise-induced spikings. Then, the global state exhibits a counterclockwise rotation on a noisy limit cycle (e.g., see the limit cycle in Fig. 1(a) for $J = 50$ μA/cm^2), and hence stochastic spiking coherence occurs. However, when passing a higher threshold J_h^* ($\simeq 141.9$ μA/cm^2), the noisy limit cycle is transformed into another noisy equilibrium point (represented by a solid circle) [e.g., see the case of $J \simeq 142$ μA/cm^2 in Fig. 1(a)], and then an incoherent state appears. As in globally coupled chaotic systems,[7–10] the mean square deviation of the global potential $V_G(t)$ (i.e., time-averaged fluctuations of $V_G(t)$),

$$\mathcal{O} \equiv \overline{(V_G(t) - \overline{V_G(t)})^2}\,, \tag{4}$$

plays the role of an order parameter used for describing the coherence-incoherence transition, where the overbar represents time averaging. Here, we discard the first time steps of a stochastic trajectory as transients for 10^3 ms, and then we numerically compute $\mathcal{O}$ by following the stochastic trajectory for 10^4 ms. For the coherent (incoherent) state, the order parameter $\mathcal{O}$ approaches a nonzero (zero) limit value in the thermodynamic limit of $N \to \infty$. Figure 1(b) shows a plot of the order parameter versus the coupling strength J. For $J < J_l^*$, incoherent states exist because the order parameter $\mathcal{O}$ tends to zero as $N \to \infty$. As J passes the lower threshold

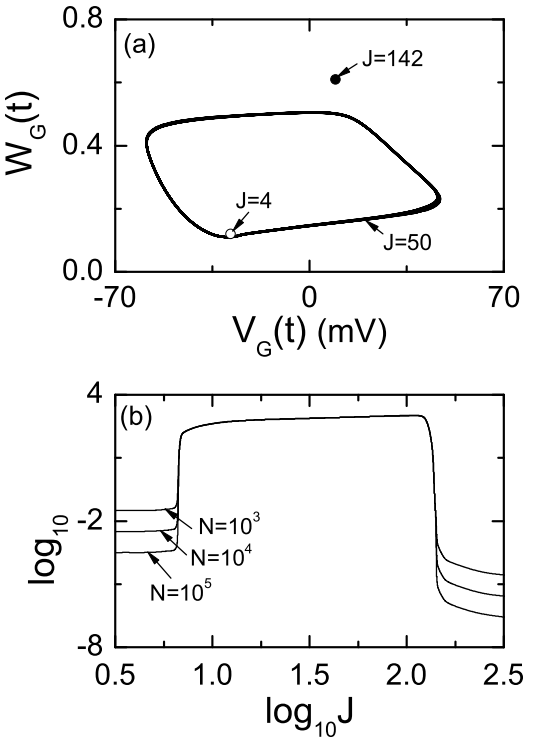

Fig. 1. (a) Coherent and incoherent states for $N = 10^3$ and $D = 1.5\ \mu\text{A} \cdot \text{ms}^{1/2}/\text{cm}^2$. Noisy equilibrium point near $(V_G, W_G) \simeq (-24.8, 0.1)$ for $J = 4\ \mu\text{A}/\text{cm}^2$, noisy limit cycle for $J = 50\ \mu\text{A}/\text{cm}^2$, and noisy equilibrium point near $(V_G, W_G) \simeq (9.3, 0.6)$ for $J = 142\ \mu\text{A}/\text{cm}^2$. (b) Plots of $\log_{10} \mathcal{O}$ versus $\log_{10} J$ for $D = 1.5\ \mu\text{A} \cdot \text{ms}^{1/2}/\text{cm}^2$.

J_l^*, a coherent transition occurs because the coupling stimulates coherence between noise-induced spikings. However, for large $J > J_h^*$, such coherent states disappear due to the effect of coupling-induced oscillator death occurring for large J (which will be discussed below).

Figures 2(a1)–2(a4) show phase portraits of the global and local output signals in the coherent regime. Since our neural network is globally coupled, any local neuron may be a representative one. By comparing the local and global phase portraits, one can obtain qualitative information about the degree of collective spiking coherence. For an optimal coupling strength J^* ($\simeq 141\ \mu\text{A}/\text{cm}^2$), the global state exhibits a collective motion on the the gray limit cycle. For this optimal case, the degree of collective spiking coherence seems to be maximal because the gray limit cycle coincides nearly with the black limit cycle of the first local state, as shown in Fig. 2(a2). However, as J is deviated from J^*, the size of the global gray limit cycle decreases [see Figs. 2(a1), 2(a3), and 2(a4)], and hence the degree of collective spiking coherence (i.e., the degree of "resemblance" of the global output signal to the local output signal) decreases. Such degree of collective spiking coherence may

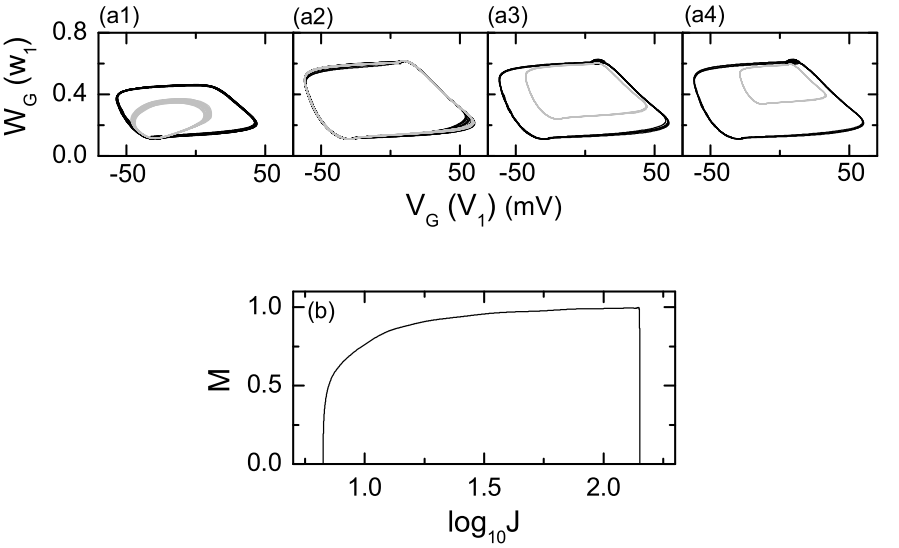

Fig. 2. Phase portraits and coherence measure for $N = 10^3$ and $D = 1.5\ \mu\text{A} \cdot \text{ms}^{1/2}/\text{cm}^2$. Gray (black) limit cycles of the global (first local) state for (a1) $J = 8\ \mu\text{A}/\text{cm}^2$, (a2) $J = 141\ \mu\text{A}/\text{cm}^2$, (a3) $J = 141.7\ \mu\text{A}/\text{cm}^2$, and (a4) $J = 141.8\ \mu\text{A}/\text{cm}^2$. (b) Plot of coherence measure M versus $\log_{10} J$.

be quantified by a measure M defined by[20,21]

$$M \equiv \frac{\sqrt{\mathcal{O}}}{\frac{1}{N}\sum_{i=1}^{N}\sqrt{\overline{(V_i(t) - \overline{V_i(t)})^2}}}\,. \tag{5}$$

This coherence measure M is just the ratio between the standard deviation (i.e., the root-mean-square deviation) of the global potential $V_G(t)$ and the population average over each neuron's standard deviation of local potential V_i (i.e., M reflects the degree of "resemblance" of the global potential to the local potential). For a coherent state, $0 < M \leq 1$, while in an incoherent state, $M = 0$. Here, we numerically compute M by following the stochastic trajectory during 200 oscillations of $V_G(t)$ after a transient process of 10^3 ms when $N = 10^3$. Figure 2(b) shows the plot of M versus the coupling strength. As J is increased from J_l^*, M increases, it becomes maximal for $J = J^*$, and then it decreases to zero abruptly for $J = J_h^*$. Such an abrupt decrease in M for $J > J^*$ results from the effect of oscillator death occurring when J is large.

Finally, we discuss the coupling-induced death of local oscillations. Figure 3(a) shows the phase portrait of the first local state (v_1, w_1) for an incoherent (firing) case of $J = 142\ \mu\text{A}/\text{cm}^2$. We note that the motion on the noisy limit cycle is strongly nonuniform because the local state (v_1, w_1) spends much time near the point of $(v_1, w_1) \simeq (9.3, 0.6)$ [i.e., the point density near $(v_1, w_1) \simeq (9.3, 0.6)$ is very high]. With increase in J, such nonuniformity of the motion along the noisy

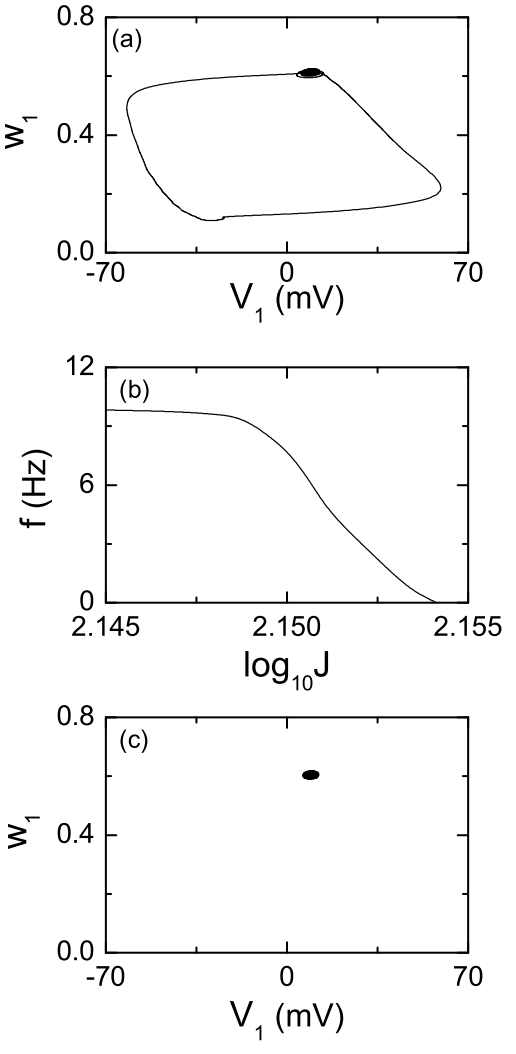

Fig. 3. Oscillator death for $N = 10^3$ and $D = 1.5\ \mu\text{A}\cdot\text{ms}^{1/2}/\text{cm}^2$. (a) Nonuniform motion of the first local state on a noisy limit cycle for $J = 142\ \mu\text{A}/\text{cm}^2$. (b) Plot of the average firing frequency f versus $\log_{10} J$. (c) Noisy equilibrium point for $J = 143\ \mu\text{A}/\text{cm}^2$.

limit cycle is intensified, and hence the average spiking frequency f decreases, as shown in Fig. 3(b). Eventually, when passing a threshold J_o^* ($\simeq 142.6\ \mu\text{A}/\text{cm}^2$), the noisy limit cycle is transformed into a noisy equilibrium point (e.g., see Fig. 3(c) for $J = 143\ \mu\text{A}/\text{cm}^2$), which is similar to the case of the saddle-node bifurcation on an invariant circle (also called the infinite-period bifurcation) in the deterministic case (without noise).[22] As a result, oscillator death (i.e., quenching of noise-induced spikings) occurs for $J > J_o^*$ because each local neuron is attracted to a noisy equilibrium state.

3. Summary

We have numerically investigated coupling-induced spiking coherence by varying the coupling strength J in an ensemble of globally coupled subthreshold ML neurons.[23] As J passes a lower threshold J_l^*, a coherent transition, which is described in terms of the order parameter, occurs because the coupling induces collective coherence between noise-induced spikings. The degree of collective spiking coherence is well-characterized in terms of a coherence measure M reflecting the degree of resemblance of the global potential to the local potential. As J is increased from J_l^*, M increases, it becomes maximal at an optimal coupling strength J^*, and then it decreases dramatically. Such an abrupt decrease in M results from the effect of oscillator death (i.e., cessation of noise-induced spikings) which occurs for large J because each neuron is attracted to a noisy equilibrium state. Through competition of these two different roles of coupling, coupling-induced spiking coherence is found to occur over a large range of intermediate coupling strength. Finally, we note that collective coherence of noise-induced spikings might be an origin for synchronous brain rhythms in a noisy environment, which correlate with the brain function of encoding sensory stimuli.

Acknowledgments

This work was supported by the Research Grant from the Kangwon National University. S.-Y. Kim thanks Prof. Yakovlev for hospitality.

References

1. G. Buzsáki, *Rhythms of the Brain* (Oxford University Press, New York, 2006).
2. C. M. Gray, *J. Comput. Neurosci.* **1**, 11 (1994).
3. X.-J. Wang, in *Encyclopedia of Cognitive Science*, ed. L. Nadel (MacMillan, London, 2003), pp. 272–280.
4. C. Morris and H. Lecar, *Biophys. J.* **35**, 193 (1981).
5. J. Rinzel and B. Ermentrout, in *Methods in Neural Modeling: From Ions to Networks*, eds. C. Koch and I. Segev (MIT Press, Cambridge, 1998), p. 251.
6. K. Tsumoto, H. Kitajima, T. Yoshinaga, K. Aihara and H. Kawakami, *Neurocomputing* **69**, 293 (2006).
7. S.-J. Baek and E. Ott, *Phys. Rev. E* **69**, 066210 (2004).
8. D. Topaj, W.-H. Kye and A. Pikovsky, *Phys. Rev. Lett.* **87**, 074101 (2001).
9. A. S. Pikovsky, M. G. Rosenblum and J. Kurths, *Europhys. Lett.* **34**, 165 (1996).
10. H. Sakaguchi, *Phys. Rev. E* **61**, 7212 (2000).
11. K. Bar-Eli, *Physica D* **14**, 242 (1985).
12. D. G. Aranson, G. B. Ermentrout and N. Kopell, *Physica D* **41**, 403 (1990).
13. G. B. Ermentrout and N. Kopell, *SIAM J. Appl. Math.* **50**, 125 (1990).
14. Z. Neufeld, I. Z. Kiss, C. Zhou and J. Kurths, *Phys. Rev. Lett.* **91**, 084101 (2003).
15. S. D. Monte, F. d'Ovidio and E. Moskilde, *Phys. Rev. Lett.* **90**, 054102 (2003).
16. The values of the parameters are the same as those in Ref. 5 except for the membrane capacitance C; more coherent states seem to appear for smaller C.
17. A. L. Hodgkin, *J. Physiol.* **107**, 165 (1948).
18. E. M. Izhikevich, *Int. J. Bifurc. Chaos* **10**, 1171 (2000).

19. M. San Miguel and R. Toral, in *Instabilities and Nonequilibrium Structures VI*, eds. J. Martinez, R. Tiemann and E. Tirapegui (Kluwer Academic Publisher, Dordrecht, 2000), p. 35.
20. D. Golomb and J. Rinzel, *Physica D* **72**, 259 (1994).
21. D. Hansel and G. Mato, *Neural Comput.* **15**, 1 (2003).
22. S. H. Strogatz, *Nonlinear Dynamics and Chaos: With Applications to Physics, Biology, Chemistry, and Engineering* (Addition-Wesley, Reading, MA, 1994).
23. W. Lim and S.-Y. Kim, *J. Korean Phys. Soc.* **51**, 1427 (2007); *ibid.* **52**, 1913 (2008); *Int. J. Mod. Phys. B* **23**, 703 (2009). The value of the noise intensity D in these references must be corrected as $D \to D * C$ by multiplying the value of the capacitance $C(= 5\ \mu\mathrm{F/cm}^2)$ (e.g., if $D = 0.3$, the corrected value is $D = 1.5$).